Geophysical Research Letters

RESEARCH LETTER
10.1029/2025GL117142

A Storyline Climate-Change Attribution Study of a High-Impact Hailstorm in Switzerland

R. J. Trapp[1], S. G. Lasher-Trapp[1], R. D. Claybrooke[1], and O. Romppainen-Martius[2]

[1]Department of Climate, Meteorology, and Atmospheric Sciences, University of Illinois Urbana-Champaign, Urbana, IL, USA, [2]Institute of Geography, University of Bern, Bern, Switzerland

Key Points:

- On 28 June 2021, a high-impact hail event occurred over parts of Europe including Zurich, Switzerland
- The geographical area covered by 3-cm or 5-cm hail in Switzerland appears to have been increased by anthropogenic climate change
- This conclusion is consistent with analyzed physical processes that govern the intensity of hail-generating storms

Supporting Information:

Supporting Information may be found in the online version of this article.

Correspondence to:

R. J. Trapp,
jtrapp@illinois.edu

Citation:

Trapp, R. J., Lasher-Trapp, S. G., Claybrooke, R. D., & Romppainen-Martius, O. (2025). A storyline climate-change attribution study of a high-impact hailstorm in Switzerland. *Geophysical Research Letters*, *52*, e2025GL117142. https://doi.org/10.1029/2025GL117142

Received 29 MAY 2025
Accepted 3 SEP 2025

Abstract We employed a "storyline" approach to explore possible anthropogenic climate change influences on the extreme hail event in Switzerland on 28 June 2021. An ensemble of factual WRF simulations with randomly perturbed initial and boundary conditions was compared to an ensemble of counter-factual simulations in which a mean climate change signal was removed from the model conditions. Using data from six GCMs, this signal was computed using differences between data averaged over current-day and pre-industrial time intervals. Relative to counter-factual simulations, factual simulations exhibited overall more hail, particularly for diameters ≥3 cm. This is consistent with increased CAPE but minimal changes in melting depth over this region in the current day. We quantified the fraction of attributable risk and concluded that the geographical areas covered by hail of diameters ≥3 and 5 cm appear to have been increased by the meteorological changes attributable to climate change.

Plain Language Summary We used high-resolution weather model simulations to investigate the likelihood that human-induced climate change contributed to extreme hail event in Switzerland on 28 June 2021. We concluded that the geographical area covered by hail of diameter larger than 3 and 5 cm appears to have been increased by the meteorological changes attributable to climate change.

1. Introduction

On 28 June 2021, an extreme hail event impacted parts of Europe including Switzerland. As documented by Kopp et al. (2023), a single-event record of 20,000 vehicle-damage insurance claims were reported by La Mobiliére, a private Swiss insurance company. In the region of Lucerne, Switzerland more than 12,000 buildings were damaged, further contributing to losses of 400 million Swiss Francs (~425 million USD in 2021) (Schmid et al., 2024). Such losses were associated with the largest areas of severe and extreme hail ever to be recorded in Switzerland since the deployment of the Swiss weather radar network in 2002. Within these areas were reports of 9-cm hailstones, which have a 70 to 100-year return period (Kopp et al., 2023).

Given the observed multi-decadal increase in meteorological conditions favoring severe-thunderstorms over Europe (Taszarek et al., 2021) and a projected further increase in these conditions into the future (Raupach et al., 2021), we are compelled to explore the possibility that ongoing climate change contributed to the anomalous and extreme nature of this hail event. The meteorological conditions of particular relevance for hailfall are convective available potential energy (CAPE), deep layer vertical wind shear, and the height of the melting level (e.g., see Mallinson et al., 2023). The general expectations are for CAPE to increase, vertical wind shear to decrease, and melting level to increase in association with climate change (Raupach et al., 2021). The extent to which these changes might be realized in terms of changes in hailfall—especially of extreme amounts and sizes—depends in part on convective storm initiation and thereafter on complex microphysical pathways of hail growth. Assessment of such realization for single events as well as for all events over multi-decadal periods is achievable via model simulations, but the spatial scales of hailstorms (~1 km to ~10s of kilometers) relative to the effective spatial resolutions of typical global and even regional climate models (GCMs, RCMs) pose methodological challenges for the attendant climate-change attribution investigations (National Academies of Sciences et al., 2016; Otto, 2023).

As demonstrated by a growing number of studies (e.g., Bercos-Hickey et al., 2021; Carroll-Smith et al., 2020; Lackmann, 2015; Lasher-Trapp et al., 2023; Mallinson et al., 2023; Martín et al., 2024; Trapp & Hoogewind, 2016; Woods et al., 2023), the modeling challenges can be overcome through use of the *event-level* pseudo-global-warming (PGW) approach (Kimura & Kitoh, 2007; Sato et al., 2007) on kilometer-scale model grids. The

PGW approach usually entails a comparison of simulations of a current-day weather event with simulations of the weather event projected into a GCM-informed future environment. Accordingly, it offers an efficient and flexible means to investigate, at high resolution and over multiple experiments, the response of a weather event to an imposed climate change (see Trapp et al., 2021). Because the imposed climate change is the focus of the experimentation, the PGW methodology also offers a straightforward separation of cause and effect.

We have used this methodology to investigate how current-day events involving tornadoes (Carroll-Smith et al., 2020; Trapp & Hoogewind, 2016; Woods et al., 2023), hail (Mallinson et al., 2023), and derechos (Lasher-Trapp et al., 2023) might be realized in a future climate. Herein we adapt the PGW methodology as a "storyline" approach for single-event attribution and investigate how the 28 June 2021 Swiss hail event might be realized in a *past, pre-industrial climate*. A comparison between an ensemble of such counter-factual simulations with an ensemble of factual simulations allows for a quantification of the fraction of attributable risk due to climate change, using relevant framing.

2. Materials and Methods

We followed the basic procedure used in our past studies, beginning with a numerical simulation of the 28 June 2021 event under its current-era, 4D state. This *reference* simulation (REF)—which provides the basis for the *factual* simulations—was performed using the Weather Research and Forecasting model (WRF) version 4.5.2 (Skamarock et al., 2021), configured with NSSL microphysics (Mansell et al., 2010), the MYJ planetary boundary layer scheme (Janjić, 1994), the RRTM short- and long-wave radiative transfer schemes (Iacono et al., 2008), the Noah land surface model (Tewari et al., 2004), 50 vertical levels, and 1-km horizontal grid lengths, which are sufficient to resolve the salient processes of the convective storms on 28 June 2021. The computational domain extended from approximately 1.5°E to 11.5°E longitude, and 43°N to 48.5°N latitude, thus enclosing Switzerland and much of the Swiss Alps. ERA5 reanalysis data (Hans Hersbach et al., 2020) provided the initial and boundary conditions (ic/bc).

Counterfactual simulations were then conducted by rerunning the reference simulation with a removal of a mean, anthropogenic climate change signal since 1850 (hereinafter ACC) from the ERA5 ic/bc. As denoted by Δ, this signal for some variable α was estimated using CMIP6 (Eyring et al., 2016) GCM data as:

$$\Delta\alpha = \overline{\alpha}_{\text{pre–industrial}} - \overline{\alpha}_{\text{historical}} \quad (1)$$

where α represents monthly mean 3D temperature (T), specific humidity (q), zonal and meridional components of wind (u, v), 2D pressure, or skin temperature. The overbars in Equation 1 indicate 10-year or 30-year averages from *historical* and *piControl* experiments in CMIP6 (Eyring et al., 2016). The specific *historical* periods are either 2005–2014 or 1985–2014; the specific *pre-industrial* periods are either the final 10 or 30 years in the GCM simulations integrated over multiple centuries to reach a stable, quasi-equilibrium state under 1850 conditions (see Eyring et al., 2016). The implications of, and justifications for different averaging periods are discussed by Trapp et al. (2021). For our study, the monthly means are specifically for the month of June, that is, the month of the hailstorm event. Once determined via Equation 1, the Δ for each variable was vertically and horizontally interpolated to the ERA5 grid, and then added to the corresponding ERA5 variable (e.g., see Equation 1 in Trapp et al., 2021); the interpolation procedure was inspired in part by Brogli et al. (2023). Given the short (30-hr) integration lengths of the simulations, we did not explicitly modify the greenhouse gas concentrations in the WRF model. We also did not modify soil moisture and soil temperature beyond their current state, owing to the lack of sensitivity of severe convective storms to imposed soil Δ′ s shown by Trapp & Hoogewind (2016).

Twelve sets of Δ′ s were computed with these two different averaging periods and data from six different CMIP6 GCMs, namely, BCC-ESM1, CanESM5, CNRM-ESM2, MIROC6, MPI-ESM1, and MRI-ESM2. These GCMs were chosen because of their availability of all required atmospheric variables for both experiments. An additional six sets of Δ's were computed using *historical* (1850–1859) rather than *piControl* experiment data for the $\overline{\alpha}_{\text{pre–industrial}}$ term in Equation 1 for each of the six GCMs. This allowed for the possibility of a different perspective of "pre-industrial" conditions; the resultant Δ fields are, however, geospatially and quantitatively similar to those using *piControl* experiment data.

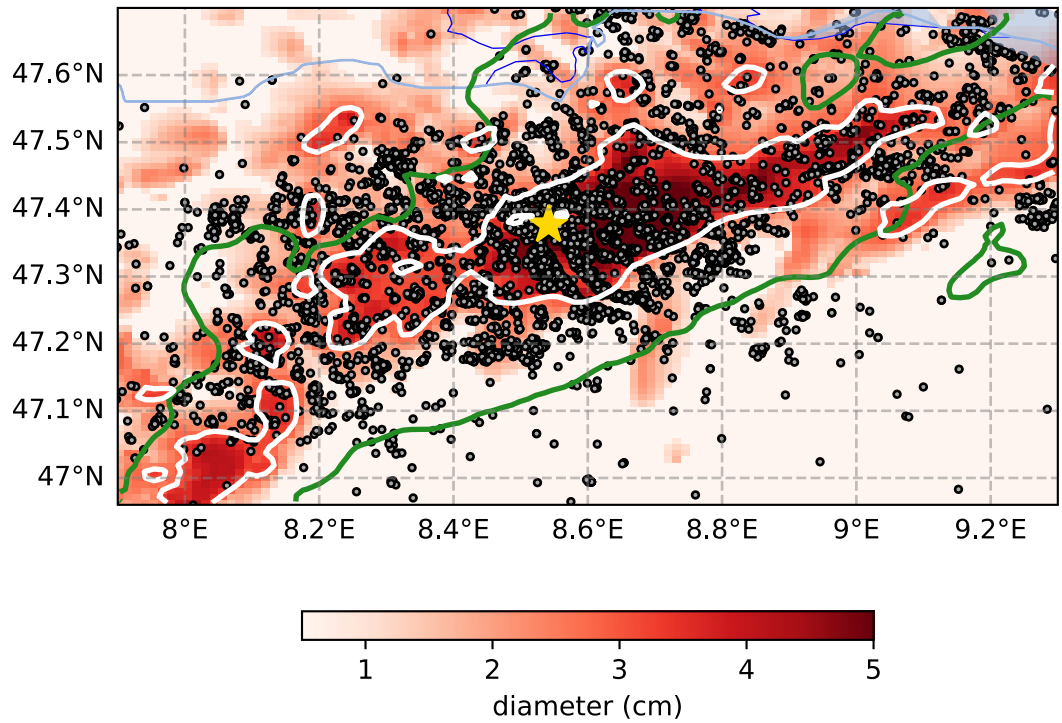

Figure 1. WRF-simulated maximum hail size over the entire model integration in a Zurich-centered subdomain for the reference simulation (color fill; cm), ≥90% probability of hail as determined from radar data collected by the Swiss radar network (green contour), and crowd-sourced hail reports of any size (dots; see Kopp et al., 2023). Gold star indicates the location of Zurich. White contour emphasizes simulated hail 3-cm or greater.

Thus, our counter-factual ensemble has a total of 18 members. For reference, the ensemble-averaged $\Delta u_{10m} \sim \pm 0.5$ m s^{-1}, $\Delta T_{2m} \sim -1$°C, $\Delta q_{850\ hPa} \sim -0.5$° g kg^{-1}, and $\Delta u_{500\ hPa} \sim -0.5$ m s^{-1} (Figure S1 in Supporting Information S1). The hypothesis based on ΔT_{2m}, $\Delta q_{850\ hPa}$, and their associations with CAPE (e.g., see Trapp, 2013), is that storms in the counter-factual environments will be weaker and therefore produce less significant hail than in the REF simulation.

Guided by these ensemble-averaged Δ's as well as by measurement uncertainty (e.g., Lin & Hubbard, 2004), we developed an 18-member ensemble of factual simulations by adding three different sets of random perturbations of ±0.5 or ±1 to, separately, T_{2m} (°C), u_{10m} (m s^{-1}), and q_{138} (g kg^{-1}) in the ERA5 ic/bc, where q_{138} indicates specific humidity at the lowest hybrid sigma level of ERA5. The hypothesis is that the randomly perturbed environments in the factual simulations will still possess the salient forcing of the REF simulation and therefore result in comparably significant hail as in the REF simulation.

3. Results

In Figure 1, a comparison between the hailfall in the REF simulation to the observed hailfall is made over a geographical area centered about Zurich, thus encompassing the area of highest economic impact and associated reported and radar-estimated hail (see Kopp et al., 2023); all analyses described henceforth apply to this geographical domain. Here, the local peak of the WRF model diagnostic *HAIL_MAXK1* over the 36-hr integration is used to represent the simulated hail swath; *HAIL_MAXK1* provides model-diagnosed hail diameter at the lowest model level, that is, near the ground. Of note in Figure 1 is the correspondence between the area of model-diagnosed hail ≥3 cm diameter (equivalent to "severe" hail in the United States) and the high density of crowd-sourced hail reports. More broadly, the total number of grid point occurrences (4570) of the radar-estimated probability of hail (POH) ≥ 90% is within 10% of the total simulated hail swath occurrences (5010) of hail ≥1-cm. This quantification is graphically illustrated in Figure 1 by the enclosure of the simulated hail swath within the contour of POH >90%. These favorable comparisons of hailfall between the observations and the

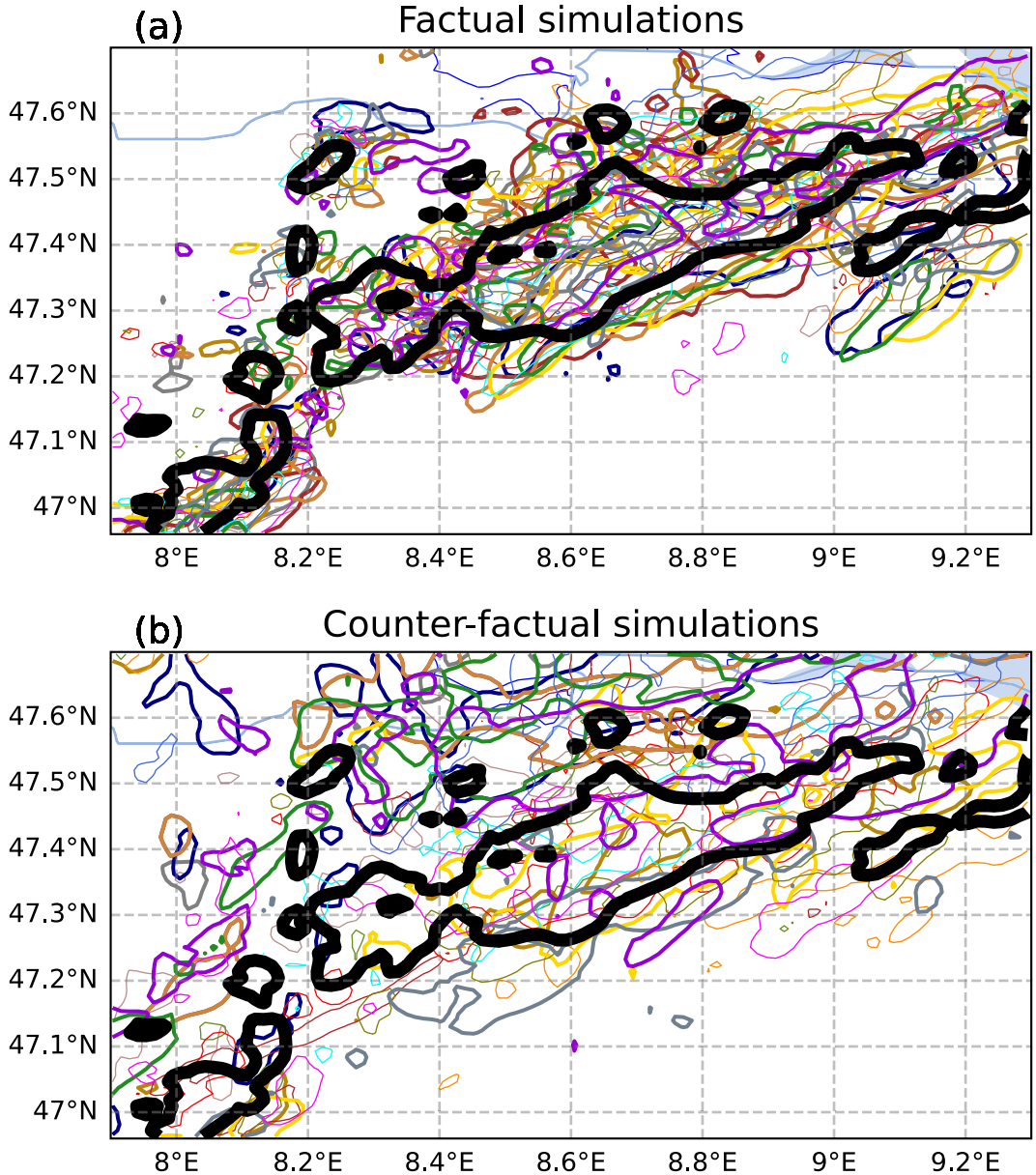

Figure 2. Contours of WRF-simulated, near-ground 3-cm hail swaths for the (a) factual ensemble members and (b) counter-factual ensemble members. The bold black contours represent the 3-cm hail swath for the reference simulation (REF). The swaths encompass all hail sizes over the entire model integration (see Figure 1).

simulation provide confidence in the representativeness of the actual hail event by the REF simulation, and thus in the subsequent analyses.

In addition to exhibiting high agreement with the REF simulation hail swath, the swaths from the individual factual simulations are geographically consistent across the ensemble (Figure 2a; see also Figure S2a in Supporting Information S1). This suggests that the meteorological forcing of this event is sufficiently strong such that when randomly perturbed, it still leads to hail-generating convective storms over roughly the same track and area (see also Figure S3a in Supporting Information S1). When the forcing is more uniformly modified, as in the counter-factual simulations by removal of the ACC signal, hail-generating convective storms are also supported within the geographical domain (Figures 2b and S3b in Supporting Information S1). However, the counter-factual hail swaths (Figures 2b; see also Figure S2b in Supporting Information S1) exhibit much more variability in area

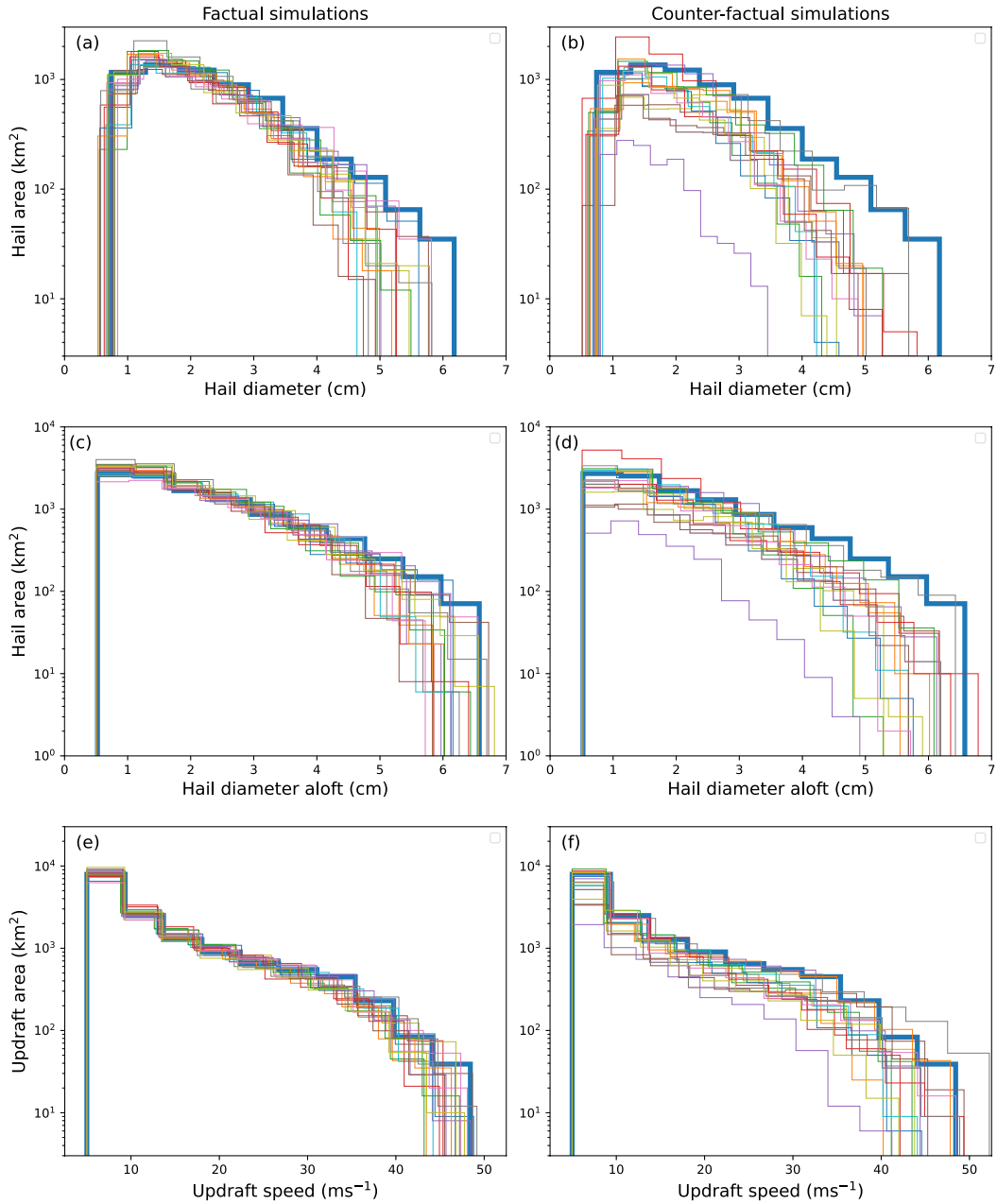

Figure 3. Histogram of cumulative area (km^2) for the factual (left column) and counter-factual (right column) simulations of: (a, b) hourly WRF-simulated maximum hail size (cm) near the ground, (c, d) hourly WRF-simulated maximum hail size (cm) aloft, and (e, f) hourly WRF-simulated maximum updraft speed (m s^{-1}) in the vertical column. Colors indicate individual simulations, with the bold line representing the reference simulation (REF). Low-end thresholds were applied to each set of analyses.

and location relative to those of the factual simulations (Figure 2a), indicating that the climate change signal is beyond random noise in the meteorological fields.

As quantified using summed areas of near-ground hail for specific diameters, we find that, relative to the REF simulation, the factual simulations exhibit a tendency for the generation of slightly larger areas of small hail, comparable areas of 2–3 cm hail, and smaller areas of the largest hail (Figure 3a). In fact, such reduced amounts of hail ≥5 cm and the complete lack of 6-cm hail in the factual simulations suggest that especially favorable conditions were required to yield these largest hail sizes in the REF simulation. Thus, our primary reference for

comparison hereinafter will be areas of hail ≥3 cm (although later we will also consider hail ≥5 cm). We find that the counter-factual simulations exhibit a tendency for the generation of smaller areas of hail at *all sizes* relative to the REF simulation, but especially for diameters ≥3 cm (Figure 3b), and with larger differences than evident within the factual ensemble (Figure 3a). Using the Mann-Whitney-U test, the differences in such areas of hail ≥3-cm between the factual and counter-factual simulations are statistically significant (p-value $\sim 10^{-6}$). The generation of less *large* hail in the counter-factual simulations is consistent with the hypothesis stated in Section 2 and thus with theoretical arguments regarding hail growth (Raupach et al., 2021). The generation of less *small* hail in the counter-factual environments is unexpected considering that the *absence* of ACC would be assumed to result in a relatively lower melting level height and thus less melting of small hail. However, the domain-averaged height of the environmental zero-degree wet bulb temperature (WBZ), which is considered to be the actual height below which hail would begin to melt, is only slightly lower in the counter-factual simulations (ensemble mean of 3,485 m) than in the factual simulations (ensemble mean of 3,577 m) (Figure S4 in Supporting Information S1), with a statistically significant difference (p-value $\sim 10^{-4}$). These small differences in WBZ between the factual and counter-factual simulations are consistent with the minor difference in the melting of small hail in the two ensembles.

One possible explanation is that all sizes of hailstones are reduced in the counter-factual environments simply because those storms were generally not as favorable for producing hail of any sizes, irrespective of melting that may occur. An evaluation of hail generation aloft via the WRF model diagnostic *HAIL_MAX2D* helps address this possible explanation (Figures 3c and 3d). As revealed by the local peaks of this diagnosed maximum hail diameter within each grid column over the 36-hr integration, the amount (area) of hail of any size in the counter-factual simulations is generally less, and often far less, than in the REF and factual simulations, especially for sizes ≥3 cm (Figures 3c and 3d). Indeed, as with hail near the ground, the differences in areas of ≥3-cm hail aloft between the factual and counter-factual simulations are statistically significant (p-value $\sim 10^{-6}$). A plausible explanation is that the area of intense updraft cores (i.e., grid points over the 36-hr integration where updraft speeds exceed 25 m s^{-1}, as diagnosed using the WRF model diagnotic *W_UP_MAX*) potentially contributing to the hail generation are also fewer in the counter-factual simulations at statistically significant levels (p-value $\sim 10^{-6}$) (Figures 3e and 3f).

Analyses of the environmental conditions at 1400 UTC, which corresponds to the time just prior to the initiation of deep convection in the model simulations, provides further insight. First, consistent with our hypothesis and with the simulated maximum updraft speeds (Figures 3e and 3f), the domain-averaged most-unstable (MU) CAPE is higher across the factual simulations (ensemble mean and standard deviation of 2164 J kg^{-1} and 17 J kg^{-1} respectively) than across the counterfactual simulations (ensemble mean and standard deviation of 1955 J kg^{-1} and 173 J kg^{-1} respectively) (Figure S5 in Supporting Information S1). The relatively high standard deviation in the counter-factual ensemble is noteworthy and reflected in the high variability of updraft speed area as well as areas of hail aloft and near the ground in these simulations. The difference in CAPE between the factual and counter-factual simulations is statistically significant (p-value $\sim 10^{-6}$), although values in both sets of simulations would be viewed as supportive of hail-generating convective storms (Barras et al., 2021). Likewise, the environmental vertical wind shear over the 0–6 km layer (S06; see Trapp, 2013) would also be viewed as supportive of hail in both sets of simulations, with domain-averaged values of 22.3 m s^{-1} and 23.0 m s^{-1} (and standard deviations of 0.25 m s^{-1} and 2.15 m s^{-1}), respectively (Figure S6 in Supporting Information S1), for the factual and counter-factual ensembles. The slightly lower S06 in the factual environments is consistent with theoretical arguments (e.g., Trapp et al., 2007) and climate model analyses (e.g., Diffenbaugh et al., 2013), although the difference in domain-averaged S06 between the factual and counter-factual ensembles is not statistically significant (p-value = 0.07). Summarizing, the factual and counter-factual environments alike supported the generation of hail in simulations of the 28 June 2021 event over Switzerland, but consistent with theory, the area of severe hailfall was more extensive in the factual simulations, or in other words, those without removal of ACC.

We can now quantify these differences between the factual and counter-factual simulations in storyline terms. Here we use the fraction of attributable risk (FAR) (Allen, 2003),

$$FAR = \frac{p_1 - p_0}{p_1} \tag{2}$$

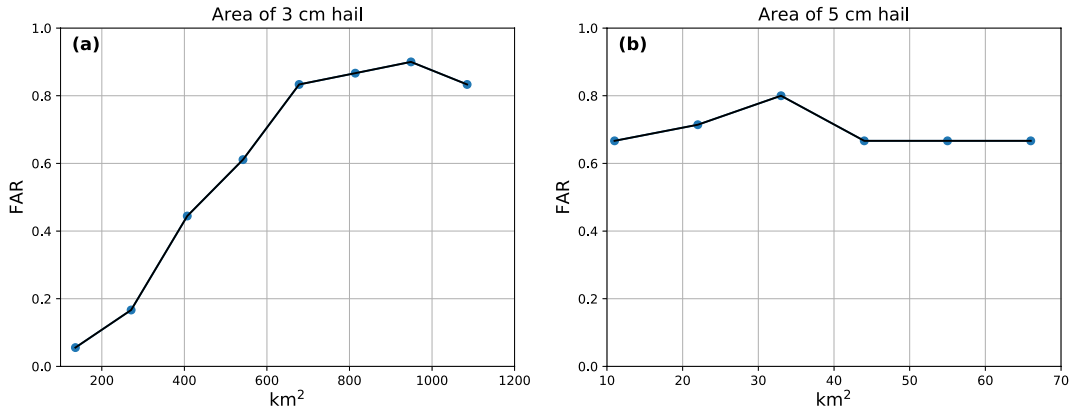

Figure 4. Fraction of attributable risk (FAR) as a function of the cumulative area of (a) 3-cm hail and (b) 5-cm hail. Probability p_1 is zero, and thus FAR is undefined, for the points not shown.

where p_1 and p_0 are, respectively, the factual and counter-factual probabilities of a specific occurrence across the relevant ensembles. There are countless ways of framing these probabilities; we used the cumulative areas of near-ground hail ≥3 cm (A_{3cm}) and ≥5 cm (A_{5cm}) (e.g., Figures 3a and 3b). For reference, the diameter threshold of 3 cm is sufficient to cause small dents in the soft metal of vehicles (Hohl et al., 2002); the diameter threshold of 5 cm (equivalent to "significantly severe" hail in the United States) can damage the windows of vehicles and destroy roof tiles (e.g., see Schmid et al., 2024). Therefore, these thresholds and associated areal metrics are relevant to the record number of vehicle- and building-damage insurance claims with this event.

We specifically used $A_{3cm,REF}$ (=1356 km^2), and $A_{5cm,REF}$ (=110 km^2), which are the areas in the REF simulation, to determine p_1 and p_0. However, because $A_{3cm} < A_{3cm,REF}$ and $A_{5cm} < A_{5cm,REF}$ for all simulations in the respective factual and counter factual ensemble (Figures 3a and 3b), we introduced a proportionality factor $\boldsymbol{\varepsilon}$ and then evaluated the counterfactual and factual probabilities as $Pr\{A_{3cm} \geq \varepsilon\, A_{3cm,REF}\}$ and $Pr\{A_{5cm} \geq \varepsilon\, A_{5cm,REF}\}$ for a range of proportionality factors, $\varepsilon = 0.1, \ldots 0.9$. Thus, the attribution is framed in terms of proportions of hail areas relative to the REF simulation.

As indicated in Figure 4, FAR has a peak value of 0.9 when the area of 3-cm hail is 949 km^2 (Figure 4a) and has a peak value of 0.8 when the area of 5-cm hail is 33 km^2 (Figure 4b). Following Hannart et al. (2016), we interpret these results to mean that given a large-scale meteorological environment like that on 28 June 2021 in Switzerland, there is a 90% probability that 3-cm hail over an area of at least 949 km^2 can be attributed to ACC, and an 80% probability that 5-cm hail over an area of at least 33 km^2 can be attributed to ACC. We can additionally interpret the smaller values of FAR in Figure 4 to mean that the probability is much lower that only small areas of these two hail categories can be attributed to ACC.

4. Conclusions and Discussion

A storyline approach using high-resolution model simulations suggests that the impact of the historic 28 June 2021 hailstorm in Switzerland was exacerbated due to anthropogenic climate change over the past 150 years. Specifically, the geographical area covered by hail of diameters exceeding 3 and 5 cm appears to have been increased by the meteorological changes attributable to anthropogenic climate change. In a highly populated city like Zurich, Switzerland and its immediate surroundings, such expanded coverage of severe hail can have disastrous consequences.

This conclusion is consistent with arguments based on the physical processes governing the intensity of hail-generating convective storms. Specifically, the CAPE prior to storm formation, and the updraft speeds within the subsequent storms, were significantly lower in the simulations without ACC. Analysis of the in-cloud hail size distribution showed that the changes in CAPE and updraft speeds were more relevant than the minor decrease in melting level height. The conclusion is also consistent with the recent results of Martín et al. (2024), who applied a similar methodology to investigate how an extreme hail event in Spain might have been realized in a pre-industrial climate.

We acknowledge that this modeling methodology, which is an adaptation of PGW, has limitations. In particular, it is a function of how the climate change signal is calculated and then removed from the meteorological forcing of the event. We chose herein to calculate this signal using differences between monthly means averaged over (near) current-day and pre-industrial time slices; this difference was meant to represent the average climate change effectively over the past 150 years. One could conceive of countless other ways to approach the calculation, including through the use of different time-averaging lengths, and/or over different time slices, and/or with constraints on days included in the time slice so that only tail conditions are represented. One could have also used additional GCMs and/or different ensemble members of the GCM experiments. Finally, different methodological approaches in obtaining and imposing the signal (e.g., Leach et al., 2024) could have been followed, if relevant to the scale of this event. Our sense based on the trajectory of our experimentation as well as on physical arguments stated in Section 2 is that the use of different climate change signals would change the details of the results but not the overall conclusion.

Despite these and the additional limitation of the computational expense of high-resolution regional model simulations, we advocate for this methodology because it offers a straightforward separation of cause and effect, which includes consideration of the underlying physical processes. We note here that for the 28 June 2021 hailstorm, the processes involving environmental buoyancy appeared to be of primary importance, but the PGW-based methodology should prove useful when other processes are dominant, including those related to convection initiation (CIN and triggering) and environmental vertical wind shear. Nevertheless, machine learning–based approaches (Trok et al., 2024) may also be an additional option for future studies. The availability of these collective tools indicates that rapid attribution studies of other extreme thunderstorm events of particular interest now seem feasible.

Data Availability Statement

The ERA5 reanalysis data used in this study are available at Hersbach et al. (2023). The GCM data sets used in this study are available through the Earth System Grid Federation (e.g., https://esgf-node.llnl.gov/projects/cmip6/), using these search criteria: Models: *BCC-ESM1, CanESM5, CNRM-ESM2, MIROC6, MPI-ESM1, and MRI-ESM2*; Experiments: *historical* and *piControl*; Ensemble: *r1i1p1*; Realm: *atmos*; and Time Frequency: *monthly*. The WRF model is available at https://www2.mmm.ucar.edu/wrf/users/, WRF namelists used to generate all simulations can be obtained at https://github.com/rjtrapp/attribution, and ic/bc files for all WRF simulation are found at Trapp (2025).

Acknowledgments
Partial support for this work was provided by the Oeschger Centre for Climate Change Research. RJT and SLT benefitted from numerous conversations with members of the Climate Impact Research Group at the University of Bern.

References

Allen, M. (2003). Liability for climate change. *Nature*, *421*(6926), 891–892. https://doi.org/10.1038/421891a

Barras, H., Martius, O., Nisi, L., Schroeer, K., Hering, A., & Germann, U. (2021). Multi-day hail clusters and isolated hail days in Switzerland – Large-scale flow conditions and precursors. *Weather and Climate Dynamics*, *2*(4), 1167–1185. https://doi.org/10.5194/wcd-2-1167-2021

Bercos-Hickey, E., Patricola, C. M., & Gallus, W. A. (2021). Anthropogenic influences on tornadic storms. *Journal of Climate*, 1–57. https://doi.org/10.1175/JCLI-D-20-0901.1

Brogli, R., Heim, C., Mensch, J., Sørland, S. L., & Schär, C. (2023). The pseudo-global-warming (PGW) approach: Methodology, software package PGW4ERA5 v1.1, validation, and sensitivity analyses. *Geoscientific Model Development*, *16*(3), 907–926. https://doi.org/10.5194/gmd-16-907-2023

Carroll-Smith, D., Trapp, R. J., & Done, J. M. (2020). Exploring inland tropical cyclone rainfall and tornadoes under future climate conditions through a case study of hurricane Ivan. *Journal of Applied Meteorology and Climatology*, *60*(1), 103–118. https://doi.org/10.1175/JAMC-D-20-0090.1

Diffenbaugh, N. S., Scherer, M., & Trapp, R. J. (2013). Robust increases in severe thunderstorm environments in response to greenhouse forcing. *Proceedings of the National Academy of Sciences*, *110*(41), 16361–16366. https://doi.org/10.1073/pnas.1307758110

Eyring, V., Bony, S., Meehl, G. A., Senior, C. A., Stevens, B., Stouffer, R. J., & Taylor, K. E. (2016). Overview of the Coupled Model Intercomparison Project Phase 6 (CMIP6) experimental design and organization. *Geoscientific Model Development*, *9*(5), 1937–1958. https://doi.org/10.5194/gmd-9-1937-2016

Hannart, A., Pearl, J., Otto, F. E. L., Naveau, P., & Ghil, M. (2016). Causal counterfactual theory for the attribution of weather and climate-related events. *Bulletin of the American Meteorological Society*, *97*(1), 99–110. https://doi.org/10.1175/BAMS-D-14-00034.1

Hersbach, H., Bell, B., Berrisford, P., Biavati, G., Horányi, A., Muñoz-Sabater, J., et al. (2023). ERA5 hourly data on single levels from 1940 to present [Dataset]. *Copernicus Climate Change Service (C3S) Climate Data Store (CDS)*. https://doi.org/10.24381/cds.adbb2d47

Hersbach, H., Bell, B., Berrisford, P., Hirahara, S., Horányi, A., Muñoz-Sabater, J., et al. (2020). The ERA5 global reanalysis. *Quarterly Journal of the Royal Meteorological Society*, *146*(730), 1999–2049. https://doi.org/10.1002/qj.3803

Hohl, R., Schiesser, H.-H., & Knepper, I. (2002). The use of weather radars to estimate hail damage to automobiles: An exploratory study in Switzerland. *Atmospheric Research*, *61*(3), 215–238. https://doi.org/10.1016/S0169-8095(01)00134-X

Iacono, M. J., Delamere, J. S., Mlawer, E. J., Shephard, M. W., Clough, S. A., & Collins, W. D. (2008). Radiative forcing by long-lived greenhouse gases: Calculations with the AER radiative transfer models. *Journal of Geophysical Research*, *113*(D13). https://doi.org/10.1029/2008JD009944

Janjić, Z. I. (1994). The step-mountain eta coordinate model: Further developments of the convection, viscous sublayer, and turbulence closure schemes. *Monthly Weather Review*, *122*(5), 927–945. https://doi.org/10.1175/1520-0493(1994)122<0927:tsmecm>2.0.co;2

Kimura, F., & Kitoh, A. (2007). Downscaling by pseudo global warming method. In *Final report to the ICCAP* (pp. 43–46). Research Institute for Humanity and Nature.

Kopp, J., Schröer, K., Schwierz, C., Hering, A., Germann, U., & Martius, O. (2023). The summer 2021 Switzerland hailstorms: Weather situation, major impacts and unique -observational data. *Weather*, *78*(7), 184–191. https://doi.org/10.1002/wea.4306

Lackmann, G. M. (2015). Hurricane Sandy before 1900 and after 2100. *Bulletin of the American Meteorological Society*, *96*(4), 547–560. https://doi.org/10.1175/BAMS-D-14-00123.1

Lasher-Trapp, S., Orendorf, S. A., & Trapp, R. J. (2023). Investigating a derecho in a future warmer climate. *Bulletin of the American Meteorological Society*, *104*(10), E1831–E1852. https://doi.org/10.1175/BAMS-D-22-0173.1

Leach, N. J., Roberts, C. D., Aengenheyster, M., Heathcote, D., Mitchell, D. M., Thompson, V., et al. (2024). Heatwave attribution based on reliable operational weather forecasts. *Nature Communications*, *15*(1), 4530. https://doi.org/10.1038/s41467-024-48280-7

Lin, X., & Hubbard, K. G. (2004). Sensor and electronic Biases/Errors in air temperature measurements in common weather station networks. *Journal of Atmospheric and Oceanic Technology*, *21*(7), 1025–1032. https://doi.org/10.1175/1520-0426(2004)021<1025:saeeia>2.0.co;2

Mallinson, H., Lasher-Trapp, S., Trapp, J., Woods, M., & Orendorf, S. (2023). Hailfall in a possible future climate using a pseudo–global warming approach: Hail characteristics and mesoscale influences. *Journal of Climate*, *37*(2), 527–549. https://doi.org/10.1175/JCLI-D-23-0181.1

Mansell, E. R., Ziegler, C. L., & Bruning, E. C. (2010). Simulated electrification of a small thunderstorm with two-moment bulk microphysics. *Journal of the Atmospheric Sciences*, *67*(1), 171–194. https://doi.org/10.1175/2009JAS2965.1

Martín, M. L., Calvo-Sancho, C., Taszarek, M., González-Alemán, J. J., Montoro-Mendoza, A., Díaz-Fernández, J., et al. (2024). Major role of marine heatwave and anthropogenic climate change on a giant hail event in Spain. *Geophysical Research Letters*, *51*(6), e2023GL107632. https://doi.org/10.1029/2023GL107632

National Academies of Sciences, Engineering, and Medicine. (2016). *Attribution of extreme weather events in the context of climate change*. The National Academies Press. https://doi.org/10.17226/21852

Otto, F. E. L. (2023). Attribution of extreme events to climate change. *Annual Review of Environment and Resources*, *48*(1), 813–828. https://doi.org/10.1146/annurev-environ-112621-083538

Raupach, T. H., Martius, O., Allen, J. T., Kunz, M., Lasher-Trapp, S., Mohr, S., et al. (2021). The effects of climate change on hailstorms. *Nature Reviews Earth & Environment*, *2*(3), 213–226. https://doi.org/10.1038/s43017-020-00133-9

Sato, T., Kimura, F., & Kitoh, A. (2007). Projection of global warming onto regional precipitation over Mongolia using a regional climate model. *Journal of Hydrology*, *333*(1), 144–154. https://doi.org/10.1016/j.jhydrol.2006.07.023

Schmid, T., Portmann, R., Villiger, L., Schröer, K., & Bresch, D. N. (2024). An open-source radar-based hail damage model for buildings and cars. *Natural Hazards and Earth System Sciences*, *24*(3), 847–872. https://doi.org/10.5194/nhess-24-847-2024

Skamarock, C., Klemp, B., Dudhia, J., Gill, O., Liu, Z., Berner, J., et al. (2021). A description of the advanced research WRF model version 4.3. https://doi.org/10.5065/1dfh-6p97

Taszarek, M., Allen, J. T., Brooks, H. E., Pilguj, N., & Czernecki, B. (2021). Differing trends in United States and European severe thunderstorm environments in a warming climate. *Bulletin of the American Meteorological Society*, *102*(2), E296–E322. https://doi.org/10.1175/BAMS-D-20-0004.1

Tewari, M., Chen, F., Wang, W., Dudhia, J., LeMone, M. A., Mitchell, K. E., et al. (2004). Implementation and verification of the unified Noah land surface model in the WRF model. *Presented at the 20th Conference on Weather Analysis and Forecasting/16th Conference on Numerical Weather Prediction, Amer. Meteor. Soc*.

Trapp, R. (2025). WRF IC/BC for hail attribution simulations [Dataset]. *Zenodo*. https://doi.org/10.5281/zenodo.15562456

Trapp, R. J. (2013). *Mesoscale-convective processes in the atmosphere*. Cambridge University Press.

Trapp, R. J., Diffenbaugh, N. S., Brooks, H. E., Baldwin, M. E., Robinson, E. D., & Pal, J. S. (2007). Changes in severe thunderstorm environment frequency during the 21st century caused by anthropogenically enhanced global radiative forcing. *Proceedings of the National Academy of Sciences of the United States of America*, *104*(50), 19719–19723. https://doi.org/10.1073/pnas.0705494104

Trapp, R. J., & Hoogewind, K. A. (2016). The realization of extreme tornadic storm events under future anthropogenic climate change. *Journal of Climate*, *29*(14), 5251–5265. https://doi.org/10.1175/JCLI-D-15-0623.1

Trapp, R. J., Woods, M. J., Lasher-Trapp, S. G., & Grover, M. A. (2021). Alternative implementations of the "pseudo-global-warming" methodology for event-based simulations. *Journal of Geophysical Research: Atmospheres*, *126*(n/a), e2021JD035017. https://doi.org/10.1029/2021JD035017

Trok, J. T., Barnes, E. A., Davenport, F. V., & Diffenbaugh, N. S. (2024). Machine learning–based extreme event attribution. *Science Advances*, *10*(34), eadl3242. https://doi.org/10.1126/sciadv.adl3242

Woods, M. J., Trapp, R. J., & Mallinson, H. M. (2023). The impact of human-induced climate change on future tornado intensity as revealed through multi-scale modeling. *Geophysical Research Letters*, *50*(15), e2023GL104796. https://doi.org/10.1029/2023GL104796